The Influence of Roughness on a High-Pressure Steam Turbine Stage: An Experimental and Numerical Study

Juri Bellucci
Department of Industrial Engineering,
University of Florence,
via di Santa Marta, 3,
Florence 50139, Italy
e-mail: juri.bellucci@arnone.de.unifi.it

Filippo Rubechini
Department of Industrial Engineering,
University of Florence,
via di Santa Marta, 3,
Florence 50139, Italy

Michele Marconcini
Department of Industrial Engineering,
University of Florence,
via di Santa Marta, 3,
Florence 50139, Italy

Andrea Arnone
Department of Industrial Engineering,
University of Florence,
via di Santa Marta, 3,
Florence 50139, Italy

Lorenzo Arcangeli
GE Oil & Gas,
via Felice Matteucci, 2,
Florence 50127, Italy

Nicola Maceli
GE Oil & Gas,
via Felice Matteucci, 2,
Florence 50127, Italy

Vincenzo Dossena
Dipartimento di Energia,
Politecnico di Milano,
via Lambruschini, 4,
Milan 20158, Italy

Introduction

The effects related to the blade surface roughness are a well-known issue for the turbomachinery designer, in particular, when dealing with the estimation of the components' performance.

The influence of surface finishing on the behavior of the adjacent flow is an aspect studied by researchers for nearly a century. The basis of these studies are the works of Nikuradse [1] and Schlichting [2], which approached the roughness-related issue in rough pipes and flat plates. On the bases of these pioneering works, many researchers have continued to study both experimen-tally and numerically the effects of surface roughness on the turbomachineries performance. A vast amount of literature on the subject is available to the turbomachinery community, likely due to many aspects that are involved with it [3,4]. Once the equiva-lent sand grain methodology proposed by Schlichting [5] was accepted, from an experimental point of view, many efforts were made to characterize surface finishing. The goal was to find an empirical correlation to convert the metrics roughness (R_a, R_t, and so on) into a sand grain (k_s) one, to employ this parameter for comparison purposes, and to fine tune closure models of numerical codes. Much progress was made in this direction, but unfortunately, because of the huge variety of surface typologies (nowadays, also analyzed by three-dimensional techniques), there is no unique correlation which solves this issue. It is worthwhile noticing that the conversion factor to obtain the sand grain roughness parameter can vary up to a factor of five, depending on the correlation adopted [3]. Some criteria use the standard metrics roughness such as the one proposed by Speidel [6] and Hummel et al. [7]. Other authors have tried to characterize the shape of the rough element and to extract a roughness density parameter to be used in their correlation. Among these, the ones proposed by Dirling [8], Sigal and Danberg [9], van Rij et al. [10], and Waigh and Kind [11] are some of the most often used.

Many other works concerned with experimental tests were performed in cascade rigs as well as in multistage environments. The goal was to provide detailed information on the effects that roughness has on the components' performance. Zhang et al. [12] studied the influence of surface roughness on the aerodynamic losses of a turbine vane, analyzing the effects of different rough surfaces (uniform and variable) and Mach number distributions. They found that losses increase with increasing exit Mach number and quantitative and qualitative different flow characteristics by varying roughness. Im et al. [13] investigated the effect of leading

Manuscript received May 9, 2014; final manuscript received July 7, 2014; published online August 26, 2014

edge roughness and Reynolds number on compressor profile loss. They found a high impact of rough blade on performance, even if 2% only of the blade pressure and suction side were rugged. This was mainly due to the influence of the rough surface on the suction side laminar separation bubble: the losses were reduced at lower Reynolds numbers and increased at the higher ones. Vázquez and Torre [14] and Hodson and Howell [15] studied the effect of surface roughness on the efficiency of a low pressure turbine. Their results suggested that in cruise conditions (high altitude), the effect of "as-cast" rough airfoils did not affect the efficiency.

The research has been active from the numerical point of view too. Many efforts were made to take into account the roughness with an appropriate wall boundary condition for the turbulence closure. In the work of Boyle [16], a numerical investigation of the effects of incidence and surface roughness was carried out, using the roughness model proposed by Cebeci and Chang. The performance of a two-stage turbine over a wide range of operating conditions was computed. A good agreement was found between computations and measurements in terms of turbine efficiency for both the smooth and the rough blades. A numerical and experimental investigation of the effects of roughness in compressor blades was carried out by Mesbah et al. [17]. They compared the results obtained with three different turbulence models, k–L, k–ω, and Spalart–Allmaras, with the measurements in terms of blade load distributions and losses. A good agreement was only found for the smooth blade. Boyle and Senyitko [18] reported an experimental and numerical analysis of surface roughness effects on a turbine vane, for four exit Mach numbers and three turbulence intensities. In their work, several metrics-to-sand grain roughness correlations were compared. Moreover, a comparison between the results obtained with the Cebeci and Chang [19] and the Wilcox roughness models were presented. Good results were obtained using the Cebeci model coupled with Mayle's [20] transition model, compared to the poor predictions obtained with Wilcox's model.

In this paper, the effects of roughness on the performance of a high-pressure steam turbine stage are investigated. In the first part of the paper, an experimental campaign conducted in a linear cascade rig is presented. The goal of the present investigation is the analysis of the combined effect of Reynolds number and surface roughness variation on blade profile losses. The total pressure loss of a vane for reaction steam turbine drums was measured with five different roughness values and in a wide range of Reynolds numbers of practical interest. The results are discussed in depth, focusing on the transitional regime of the measured flow and on the choice of the metrics-to-sand grain roughness conversion fac-tor. In the second part, details of the numerical approach are given. The roughness model is described together with the transi-tion/turbulence model used for the computations, and their valida-tion using a flat-plate flow is shown. The accuracy of such models is then tested against measurements, thus allowing for their fine-tuning and proving their reliability. Finally, three-dimensional unsteady CFD analyses are carried out on a high-pressure stage, in order to investigate the influence of roughness on the losses over the entire stage operating envelope. The time-averaged total pressure losses at midspan are compared with the profile loss coefficient computed using Craig and Cox correlation and the cascade measurements. Unsteady effects that may affect the influence of the roughness, such as the incoming wakes on the rotor blade, are taken into account, and the impact of transition-related aspects on the losses is discussed.

Experimental Measurements

Test Rig. The experimental investigation was carried out in the blow-down facility for linear cascades located at the Laboratorio di Fluidodinamica delle Macchine at Politecnico di Milano. This is a transonic wind tunnel with a test section of 80 mm height and 470 mm wide, fed by 6000 kg of pressurized air stocked at 200 bar. For the aim of the present research, the cascade was com-posed of nine blades (Fig. 1). Several repetitions (5–10) of the same test were performed to have a wider statistic analysis and reduce measurement uncertainty. The periodicity condition was achieved by means of a movable tailboard located downstream of the cascade: the differences in flow field measured downstream of the central passages were found to be within the measurements accuracy. The blade geometry represents a typical stator employed in reaction stages of high/intermediate pressure steam turbines. The blades were scaled up, in order to obtain the best compromise between Reynolds number range (based on chord and exit velocity) and cascade aspect ratio (about $AR = 1.3$).

The Reynolds number variation was obtained by pressurizing the test section in the range from 1 to 3.5 bar, by means of a variable sonic throat located at the outlet section of the wind tunnel. To guarantee an independent fine-tuning of both Reynolds and

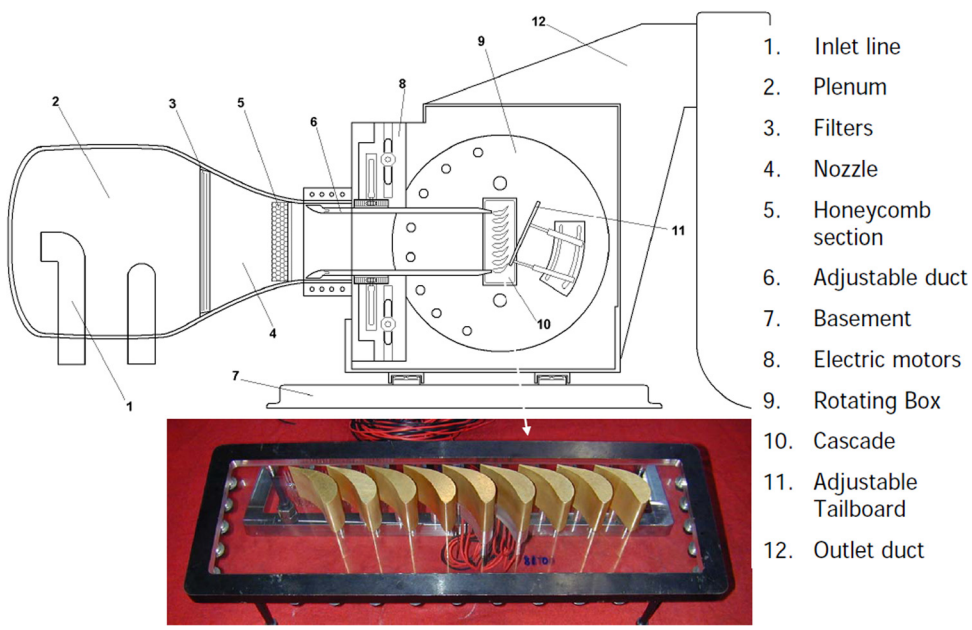

Fig. 1 Experimental test section scheme

Mach numbers, an 8 in. butterfly valve and a 2 in. regulation valve were installed. The whole range of Reynolds numbers from 0.7×10^6 to 2.5×10^6—characteristic of typical steam turbines blades of different sizes—was covered by means of 10–20 points for each surface roughness considered. Data reported here have been collected at the same expansion ratio—i.e., at a downstream isentropic Mach number of approximately 0.5—irrespective of the Reynolds number. The cascade inlet flow angle was set in order to have nominal incidence on the blade. A summary of experimental conditions and cascade data are reported in Tables 1 and 2.

Detailed measurements of the flow field downstream of the cascade have been performed by traversing at midspan a miniaturized five-hole probe (head of 1.8 mm) at a distance of 50% of the blade axial chord. The five-hole probe measurement grid was defined by 50 points spaced equally (approximately 1 mm) along a single blade passage. The five-hole probe was pre-aligned to the downstream pitchwise mass averaged flow angle evaluated at atmospheric back pressure condition. The central hole of the downstream probe was connected to a very high accuracy differ-ential pressure transducer. It was directly coupled on the reference side to the upstream total pressure line supplied by a three-hole probe located one axial chord upstream of the cascade. Since the maximum local flow angle variation downstream of the blades in all the tests with respect to the probe pre-alignment was $\pm$ 1 deg, the total pressure coefficient of the five-hole probe was always null (i.e., the correction to be applied on the pressure reading of the central hole to obtain the local flow total pressure is null). This means that the central hole pressure reading was coincident with the local actual total pressure of the flow. In these operating con-ditions, the uncertainty of the local total pressure drop measure-ment is dramatically reduced, since only the differential pressure transducer uncertainty is involved in the measurement chain, thus excluding the uncertainty involved in the whole probe calibration process. Moreover, previous research on the effect of Reynolds number variation on the calibration coefficients of the five-hole probe type used here evidenced a null influence in the Reynolds and angular range experienced in the present measurements campaign. As a result, the uncertainty in the measurement of the profile pressure loss coefficient Y ranges approximately from 0.11×10^{-2} (confidence level of 95%) when the cascade downstream pressure was set at atmosphere ($\mathrm{Re} \simeq 0.75 \times 10^6$), to 0.035×10^{-2} when the cascade downstream pressure was set at 3.5 bar ($\mathrm{Re} \simeq 2.4 \times 10^6$). The total pressure loss evaluation repeatability for a given Reynolds number and surface roughness was always found to be lower than 50% of the correspondent measurement uncertainty. More details about the experimental facility and the measurement technique can be found in Refs. [21] and [22].

The surface roughness variation was obtained by a progressive machining of the blades, by means of shot-peening using microspheres of different diameters. Thus, five roughness values ranging from $k_s/C = 0.4 \times 10^{-4}$ to 2.5×10^{-4} were considered in the frame of the present work. The smallest one can be considered equivalent to the finish of a smooth blade. The conversion factor between metrics R_t and equivalent sand grain roughness k_s was defined, as suggested by Speidel [6] and Schlichting [2], by

$$k_s = \frac{R_t}{2.56} \tag{1}$$

More details about the roughness and the shot-peening procedure are reported in Table 3.

Table 1 Cascade experimental conditions

Total pressure	1–3.5 bar
Total temperature	250–295 K
Isentropic exit Mach	0.50
Reynolds number	0.7×10^6 to 2.5×10^6
Turbulence intensity	$\simeq$1%

Table 2 Cascade data

Aspect ratio	1.3
Flow deflection	73 deg
Zweifel number	0.70

Finally, in order to complete the boundary conditions required for CFD computations, total temperature, flow angle, and turbulence intensity (estimated $Tu \simeq 1\%$) at the cascade inlet were also measured.

Results. The experimental results were available in terms of blade loading and mass averaged total pressure loss coefficient Y, defined as

$$Y = \frac{P_{t1} - P_{t2}}{P_{t2} - P_{s2}} \tag{2}$$

The campaign was mainly focused on the investigation of the surface roughness effects on the profile losses; hence, the measurements were performed at cascade midspan. The blade loading was measured for the smooth blade only, which is before shot-peening.

Experimental results are summarized in Fig. 2, where the loss coefficient is reported as a function of Reynolds number for all the investigated k_s/C. In this plot, as well as for the other succes-sive plots, losses are normalized with respect to the value at $\mathrm{Re}_2 = 1 \times 10^6$ and $k_s/C = 1.6 \times 10^{-4}$. The shape of the curve for lower k_s/C suggests that the campaign was carried out in a range of Reynolds number for which the boundary layer over the blade surface is laminar for a large part of the suction side. In fact, the trend is very close to the $\mathrm{Re}^{-0.5}$ curve, which represents the loss trend of a laminar boundary layer.

Looking at the other curves, increasing the surface roughness shifts the critical Reynolds ($\mathrm{Re}_{2,cr}$) toward smaller values. Here, $\mathrm{Re}_{2,cr}$ is defined as the value at which the loss curves start to differ from the laminar trend. The sudden increase in the profile loss is due to boundary layer laminar-to-turbulent transition, and the shape of this increase depends on the combined effect of $\mathrm{Re}_{2,cr}$ and k_s/C: lower roughnesses lead to a mild increase and vice versa. This scenario suggests that most of the data lie in a region where the boundary layer is mainly transitional. For the highest roughnesses only, the fully rough regime is reached for the highest Reynolds number. These considerations are similar to the results found by Boyle and Senyitko [18] in their cascade test rig by varying surface roughness. In their study, wide regions of laminar flow were found too, in particular, for the smooth blade case. Moreover, these results are in line with the statement of Bons [3], whereby in a clean/quiet wind tunnel it is possible to obtain a transition Reynolds number of about 3×10^6.

Similar considerations on the transitional nature of these experiments can be inferred from Figs. 3 and 4. Profile losses are shown as a function of k_s/C and Re_{2,k_s} in Figs. 3 and 4. In both plots, each curve is associated with a different Reynolds number value: for the sake of clarity only, the most significant Reynolds numbers are reported. In Fig. 3, the plot shows a region of low and quite constant losses for the lowest roughnesses (laminar boundary layer). A steep increase in the loss coefficient is found when both

Table 3 Shot-peening microspheres features

k_s/C	Diameter (mm)	Material
0.4×10^{-4}	0.21–0.3	Ceramic
0.8×10^{-4}	0.21–0.3	Ceramic
0.9×10^{-4}	0.21–0.3	Ceramic
1.6×10^{-4}	0.4	Steel
2.5×10^{-4}	0.4	Steel

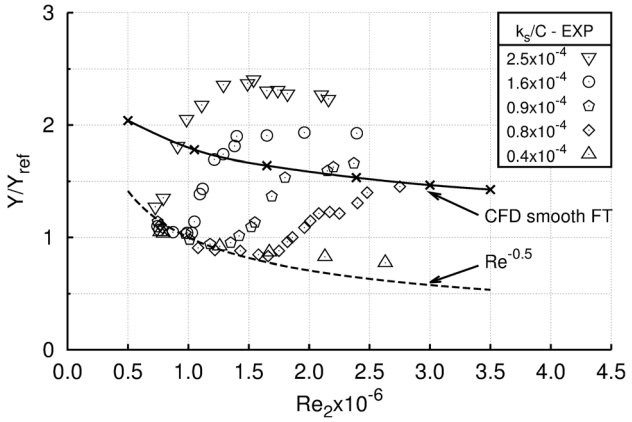

Fig. 2 Experimental total pressure loss coefficient

k_s/C and Re_2 are increased, corresponding to the trigger of boundary layer transition. Then, a substantial loss independence from the Reynolds number is observed. These trends are similar to the ones found by Speidel [23] by means of an experimental cam-paign carried out in a linear cascade, and rediscussed by Schlicht-ing [5]. In that case, the discussion was mainly focused on the impact of blade pressure distribution on boundary layer transition for different roughness values. As found in the present work, the results pointed out wide regions of laminar flow over the blade in cascade conditions. Figure 4 allows an estimation of the Reynolds whereby the transition is induced by roughness of about $\mathrm{Re}_{2,k_s,\mathrm{cr}} = 130$. This value is in good agreement with the one proposed by Feindt [24] and suggests that the conversion factor from R_t to k_s of 2.56 used is reasonable for the present case.

Computational Framework

The Flow Solver. The TRAF code [25] was used in the present work. The unsteady, three-dimensional, Reynolds-averaged Navier–Stokes equations are written in conservative form in a curvilinear, body-fitted coordinate system and solved for density, absolute momentum components, and total energy. A dual-time-stepping method [26,27] is used to perform time-accurate calculations.

Transition and Turbulence Modeling. Wilcox's classic low-Reynolds number k–ω model [28], widely used in turbomachinery calculations, is applied in combination with the laminar kinetic energy (LKE) model, which enables to take into account the pre-transitional rise of the fluctuating kinetic energy [29,30].

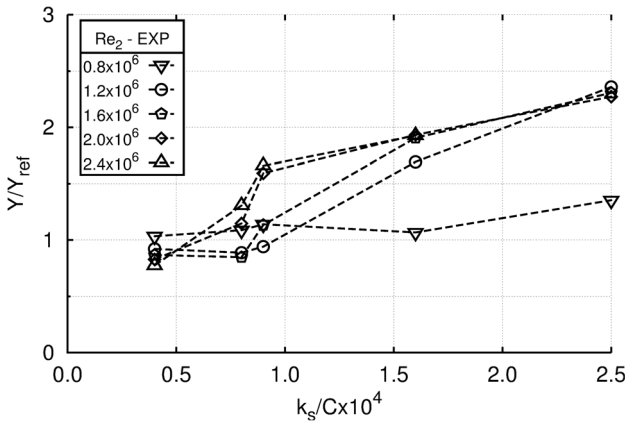

Fig. 3 Experimental total pressure loss coefficient as a func-

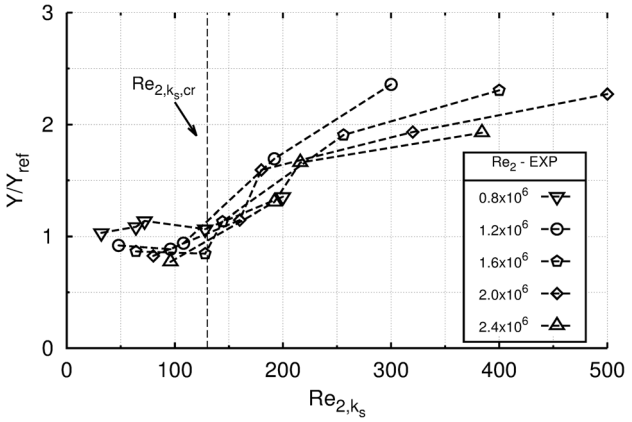

Fig. 4 Experimental total pressure loss coefficient as a function of Re_{2,k_s} for several Reynolds numbers

The laminar and turbulent kinetic energy equation can be written as follows:

$$\frac{Dk_\ell}{Dt} = P_\ell - 2\nu\frac{k_\ell}{y^2} + \nu\nabla^2 k_\ell - R \tag{3}$$

$$\frac{Dk}{Dt} = P_k - \beta^* k\omega + \frac{\partial}{\partial x_j}\left[(\nu + \sigma_k\nu_\mathrm{T})\frac{\partial k}{\partial x_j}\right] + R \tag{4}$$

where $\beta^* = 0.09$ and

$$R = C_2(1 - e^{-\psi/C_3})\omega k_\ell \tag{5}$$

is a function used to transfer energy from k_ℓ to k, $\psi = \max(R_y - C_4, 0)$ is a transition parameter based on the wall-normal-distance Reynolds number R_y, $C_2 = 1.0$, $C_3 = 8$, and $C_4 = 10$. The production term of the LKE is $P_\ell = \nu_\ell S^2$, where S is the shear rate and ν_ℓ is the "laminar eddy-viscosity," which is modeled as follows:

$$\nu_\ell = C_1\sqrt{k_\ell}\delta_\Omega \tag{6}$$

with $C_1 = 1$. For details on the implementation, see Refs. [30] and [31].

The inlet conditions for k and ω are obtained from the prescribed values of free-stream turbulence intensity $k_\infty = \frac{3}{2}Tu_\infty^2 u_\infty^2$, and turbulence length scale $\omega_\infty = k_\infty^{1/2}/\ell_{\mathrm{T}\infty}$. The inlet condition for k_ℓ is as follows: $k_{\ell\infty} = k_\infty$ (see Ref. [29] for more details). All the computations were carried out using this three-equation $k_\ell - k - \omega$ model.

Surface Roughness Model. According to Wilcox [28,32] at the wall $k_\mathrm{w} = 0$ and the value of ω is modified in order to account for the effects of surface roughness

$$\omega_\mathrm{w} = \frac{v^{*2}}{\nu_\mathrm{w}} S_\mathrm{R}; S_\mathrm{R} = \begin{cases} 4\lambda_\mathrm{R}^2 & , \quad k_\mathrm{s}^+ \le 5 \\ \lambda_\mathrm{R} + \left(4\lambda_\mathrm{R}^2 - \lambda_\mathrm{R}\right)e^{(5-k_\mathrm{s}^+)} & , \quad k_\mathrm{s}^+ > 5 \end{cases} \tag{7}$$

where v^* is the friction velocity, $k_\mathrm{s}^+ = k_\mathrm{s}v^*/\nu$ is the roughness height in wall units, and $\lambda_\mathrm{R} = 100/k_\mathrm{s}^+$.

Flat-Plate Validation. The model validation was carried out on a uniformly roughened flat plate of length L with zero pressure gradient. The computational domain extends $0.3L$ upstream of the plate leading edge. The gap between the upper and the bottom wall is $0.3L$. A mesh of 241 streamwise × 121 nodes expanding from the wall to free-stream is adopted for all the cases. The fluid is treated as incompressible, with a density of 1.2 kg/m^3 and a

Table 4 Rough flat-plate cases

Case	k_s/L	k_s^+ range	Regime
1	1×10^{-4}	21–35	Transitional
2	2.5×10^{-4}	60–100	Transitional-rough
3	5×10^{-4}	125–215	Fully rough
4	10×10^{-4}	267–450	Fully rough
5	15×10^{-4}	422–745	Fully rough

molecular viscosity of 1.8×10^{-5} Pa s, resulting in a plate Reynolds number $\mathrm{Re}_L = 5 \times 10^6$.

Five different surface roughnesses were selected for which the boundary layer status ranges from transitional to fully rough regime [5,33] (Table 4). The computation of rough-wall flows may be extremely demanding in terms of grid density: as a matter of fact the higher the roughness height is the higher the boundary layer thickness is, resulting in steeper flow gradients near the wall with respect to the smooth-wall case.

This is confirmed by many authors, who demonstrated that Wilcox's roughness model requires a very fine near-wall mesh resolution [33–35], due to the fact that the wall boundary condition for the turbulence kinetic energy is $k_w = 0$. As shown in Fig. 5 for the smooth wall, the turbulent kinetic energy k^+ rapidly decreases going toward the surface due to the presence of the viscous sublayer, and nearly vanishes for $y_1^+ \simeq 1$. The roughness suppresses the laminar sublayer, and much smaller values of the y_1^+ are mandatory in order to accurately resolve the near-wall behavior of the turbulence kinetic energy.

For this reason, a grid sensitivity analysis was carried out in which the grid spacing of the first node from the wall (y_i) was progressively halved. The results are presented in Fig. 6 in terms of drag coefficient $C_D = \int_L C_f dx$, which includes the effects of the laminar part of the boundary layer, and skin friction coefficient at $x = 0.5\ L$ for the case $k_s/L = 5 \times 10^5$, with respect to a grid refinement index y_i/y_{ref} (where y_{ref} is the finest spacing). Five grid spacings were used corresponding to y_1^+ measured at $x = L$ ranging from 1.55 to 0.05. In order to minimize round-off error linked to the use of very small spacings, double-precision results are presented.

The computed skin friction coefficients for the rough cases of Table 4 are compared with the Mills and Hang [36] correlation formula for fully rough regime (Fig. 7)

$$C_f = [3.476 + 0.707 \ln(x/k_s)]^{-2.46} \tag{8}$$

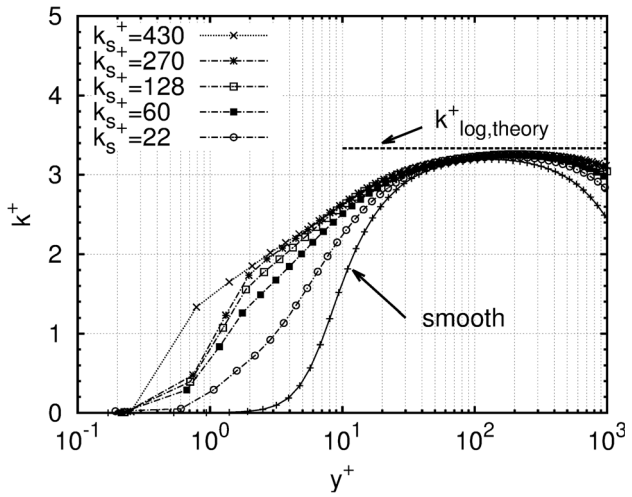

Fig. 5 Flat-plate near-wall behavior of the turbulent kinetic energy in wall units $k^+ = k/v^{*2}$, ($k^+_{log,theory} = 1/\sqrt{\beta^*}$, $\beta^* = 0.09$)

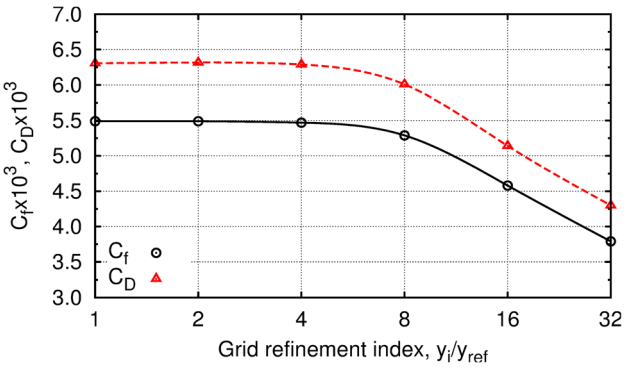

Fig. 6 Flat-plate environment: convergence of the skin friction and drag coefficients ($k_s/L = 5 \times 10^{-4}$)

Results of Fig. 7 show a good agreement for the transitional case too (case 1).

Numerical Results

Cascade Environment. The experimental data obtained for the cascade were used to fine tune the roughness model previously validated on a flat plate. The goal of the calibration was to improve the model's capability of predicting roughness-transitional flows, thus allowing to eventually use this model for predicting the impact of roughness in an actual stage environment.

Three-dimensional viscous steady runs were performed in order to match the experimental measurements. According to the mesh requirements found during the model validation, a $340 \times 64 \times 72$ O-type grid (Fig. 8) with a $y^+ \simeq 0.1$ was used.

A first comparison between experiments and computations concerns the blade loading of the smooth blade. Figure 9 shows a substantial agreement between the test rig environment and computational one.

The model calibration was started from the measurements at $k_s/C = 1.6 \times 10^{-4}$, for which laminar, transitional, and fully rough flow regimes are successively encountered at increasing exit Reynolds numbers. A parametric study was carried out in order to calibrate the numerical transition by varying the model constant $C1$ (see Eq. (6)). This parameter controls the LKE pro-duction, playing a role of crucial importance in determining the $\mathrm{Re}_{2,cr}$ that triggers the transition, and the consequent loss increase. The analysis led to the correlation reported in the following equation:

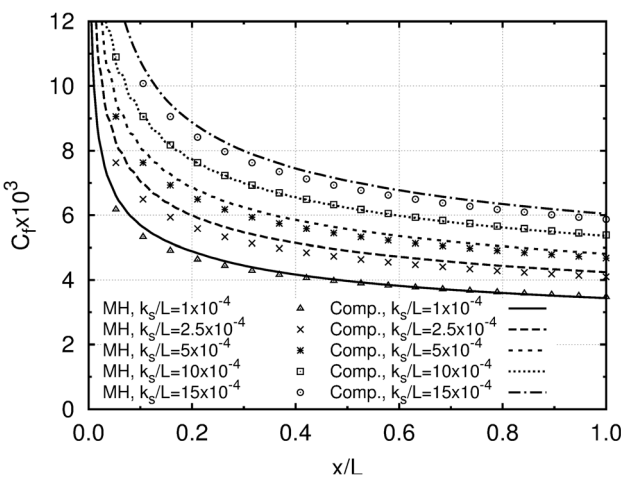

Fig. 7 Flat-plate environment: computed skin friction coefficients compared with the correlation of Mills and Hang [36]

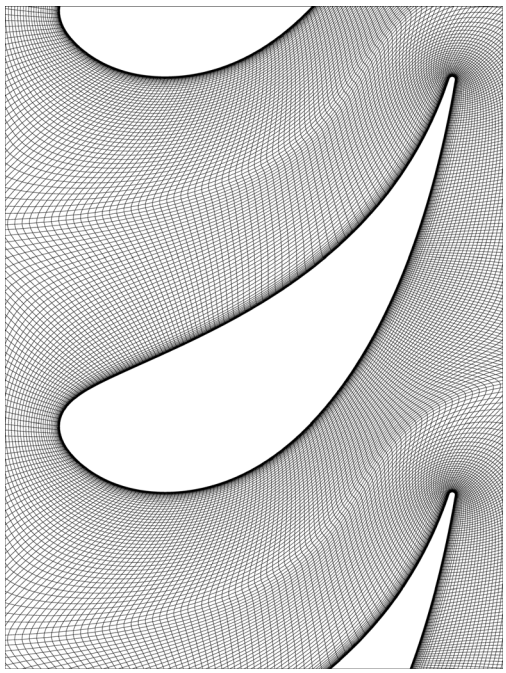

Fig. 8 Cascade two-dimensional O-type grid

$$C_1 = f_1(k_s^+) = \max\left\{0.8, 2\tanh\left[\left(k_s^+/18.13\right)^{2/3}\right]\right\} \qquad (9)$$

Such a tuning was extended to all the tested surface roughnesses, and the results are summarized in Fig. 10. The comparison shows a generally good agreement; in particular, the Re_{cr} and the subsequent increasing of losses are well predicted. The computations confirm wide region of laminar flow for $\mathrm{Re}_2 < \mathrm{Re}_{2,cr}$. For higher values, the boundary layer undergoes the laminar-to-turbulent transition and the extension of the turbulent portion grows with the Reynolds number. Thus, a quasi-fully rough regime can be considered to be reached at higher Re_2, in particular, for the higher values of k_s.

Looking at Fig. 10, two considerations can be raised. The first one concerns the transitional flow region. Fixing the value of the Reynolds number, the increase of losses while increasing k_s/C depends on two phenomena which act at the same time: the first concerns the augmentation in losses due to the rough surface, while the second one is linked to the boundary layer transition. The combination of these two aspects yields a sudden increase in the profile loss, up to 1.5–2 times depending on the case. The

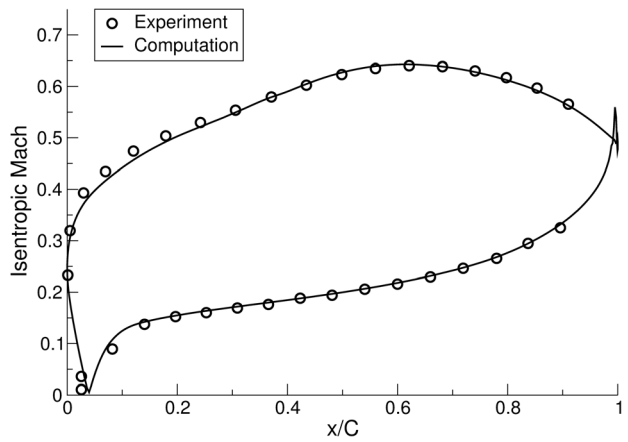

Fig. 9 Smooth blade experimental and computational isentropic Mach distribution

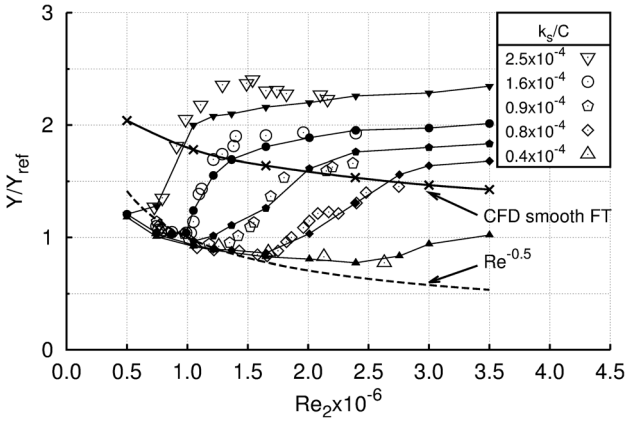

Fig. 10 Total pressure loss coefficient: experimental (open symbol) and CFD (filled symbol and solid line) results

second consideration concerns the turbulent region. The effect of transition on losses is negligible and only the roughness variation is accountable for loss increases. That is, this augmentation has to be comparable to the one estimated in a fully rough regime. CFD results predict a ratio between the loss coefficient Y (at highest Re_2 and k_s/C) and the one for the smooth surface in fully turbu-lent condition Y_{smooth} of about 1.58. This result is in very good agreement with the value of $Y/Y_{\mathrm{smooth}} \simeq 1.55$ obtained with the correlation of Craig and Cox [37], which is widely used for turbomachinery applications. Similar results are found by using the correlations proposed by Aungier [38].

Real Stage Environment

The proposed numerical framework was successively used to carry out a comprehensive CFD analysis of a high-pressure steam turbine stage. The goal was to investigate the influence of roughness on the losses over the whole stage envelope.

With respect to the cascade measurements, the actual stage environment adds some important aspects that may affect the profile losses: potential effect from upstream/downstream rows, higher free-stream turbulence intensity, and wakes from the previ-ous rows. All these perturbations can affect the boundary layer laminar-to-turbulent transition and influence how the rough surface affects the losses.

The stage investigated was composed of prismatic rows. The blade geometry used during the experimental campaign was employed for both the stator and the rotor rows. The inlet boundary conditions measured during cascade tests were adopted for the

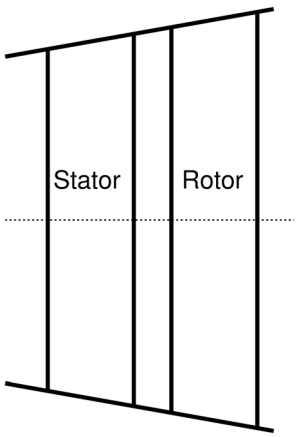

Fig. 11 Stage meridional view

computations (P_t, T_t, and Tu), while the back pressure was changed, in order to have an exit Mach number of about 0.50 for both the rows (Table 1). The stator inlet flow angle was chosen to have nominal incidence on the blade, while the value of the rota-tional speed assures the same incidence on the rotor row. For the blades axial gap, a typical value employed in a real machine lay-out was selected (about 0.4 stator C_{ax}). The meridional channel geometry has a constant mean radius, and it is slightly conical in order to ensure the same axial velocity in both the rows (Fig. 11). In this way, the midspan sections of the two blades work at the same conditions as for the cascade tests. Moreover, an aspect ratio of about $AR = 3.2$ and a radius ratio of about $RR = 1.3$ were cho-sen in order to ensure a two-dimensional flow in these sections. All the runs were performed at the same expansion ratio, while the Reynolds number varies within the range investigated experi-mentally. Moreover, the same five values of surface roughness tested were considered.

Three-dimensional viscous unsteady runs were performed, employing a full-annulus approach. Due to the high computational costs of the unsteady runs, stator and rotor blades have the same blade count, resulting in a periodicity domain of 1:1. The number of time-steps was selected after a sensitivity analysis carried out using three different values: 25, 50, and 100. Fifty time-steps per blade passing period ensured the independence of the solutions from time-steps. The O-type grid used for the cascade computa-tions was adopted for the two-row discretization (Fig. 8). A sum-mary of computational data of the stage is reported in Table 5.

The total pressure loss coefficients at the midspan section of both the stator and the rotor rows were calculated from the time-averaged solution. The data were collected in order to compare the results with the ones obtained for the cascade. The analysis of the results leads to different conclusions for the two rows. Employing the same boundary conditions of the cascade tests, the stator still works in a cascadelike environment. The boundary layer shows a laminar behavior for large part of the suction side even at the higher values of the Reynolds number, in particular, for the lower values of k_s/C. Then, as it happens for the cascade flow, a transitional behavior is found for the higher surface rough-ness and Reynolds number values. For the investigated case, with a subsonic exit flow, the presence of a blade row, which generates a potential field downstream, has a negligible effect on the genera-tion of profile losses. As far as the rotor is concerned, the trend of profile losses depicts a different scenario. The periodic impact of the wakes near the leading edge region of the rotor promotes the boundary layer transition. Most of the suction side surface is affected by turbulent flow, which results in a higher loss level compared to the steady state cascade environment with attached boundary layer. This behavior is independent of the surface finish-ing of the blade, and starts from the lowest Reynolds investigated. The results of the computations are summarized in Fig. 12, where the rotor profile losses are reported as a function of Re_2 for all the five roughnesses (filled symbol and solid line). In all the cases, the loss trend with respect to Reynolds is very close to the $Re^{-0.2}$ curve, which represents the loss trend of a turbulent boundary layer. This is the reason why the loss level is about twice the one found with the cascade experimental campaign (Y_{ref} is the same for the two cases). The figure shows how increasing k_s/C has the main effect of moving the loss curve toward higher values. More-over, it modifies the value of the threshold Reynolds (Re_{th}) at which the curve leaves the turbulent trend: the higher the rough-ness, the lower the Re_{th} value. Once the Re_{th} is overcome,

Table 5 Stage data

Axial gap	0.4 C_{ax}
Aspect ratio	3.2
Radius ratio	1.3
Periodicity domain	1:1

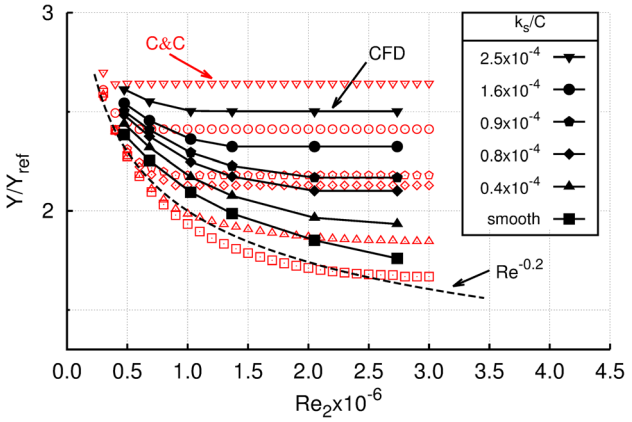

Fig. 12 Time-averaged CFD (filled symbols) and Craig and Cox correlation (open symbols) loss coefficient as a function of Re_2 (rotor row)

increasing Re_2 leads the losses trend toward the fully rough re-gime. With respect to the cascade results, the ratio between Y (at highest Re_2 and k_s/C) and Y_{smooth} is slightly lower, about 1.45. In the same plot, the loss coefficients calculated by means of the Craig and Cox correlation (open symbol) are reported. The com-parison with the CFD shows a generally good agreement. As for the cascade tests, the correlation predicts an increase of losses in fully rough regime of $Y/Y_{smooth} \simeq 1.55$. In this case, the computa-tions slightly under predict the roughness effect. Analyzing the plot, a slight shift in the absolute value is seen for all the Reynolds and surface finishing computed. In particular, when comparing to Craig and Cox's predictions, the calculations compute a higher loss at the lower k_s/C, and underestimate it at higher ones. But the main difference is in the estimation of Re_{th} and, as a consequence, of the Reynolds number at which the fully rough regime starts. Figure 13 shows the time-averaged profile losses as a function of k_s/C for different Reynolds numbers. In light of the previous dis-cussion both the CFD (black filled symbol and solid line) and the Craig and Cox (red open symbol) results show a turbulent nature. In this case, the loss trend does not present the typical "knee" of the transition region, but follows a quite linear trend, in accord-ance with Speidel's [23] results. From this point of view, the com-parison between the CFD and the correlative approach is encouraging. In fact, despite the difference in the absolute values, the slope of the curves is in good agreement with the experiments too.

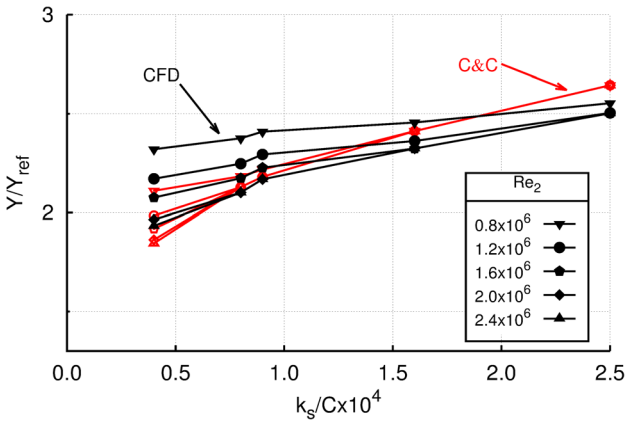

Fig. 13 Time-averaged CFD (filled symbols) and Craig and Cox correlation (open symbols) loss coefficient as a function of k_s/C (rotor row)

Summary and Conclusions

The study of the influence of surface roughness on a high-pressure steam turbine stage was the scope of the present work.

The results of an experimental campaign, conducted in a cascade test rig, were the basis for the calibration of the roughness model used in the successive calculations. The measurements were performed for five surface roughnesses and in a range of Reynolds number of industrial interest. The results were available in terms of blade loading and total pressure loss coefficient. The analysis of the data highlighted the effect of roughness on boundary layer transition, and the associated profile losses increase. The computed losses as a function of Re_{2,k_s} confirmed that the metrics-to-sand grain roughness conversion factor was reasonably selected.

Three-dimensional steady state CFD computations were performed in the cascade environment. The $k_\ell - k - \omega$ turbulence model used for the computations was calibrated in order to account for roughness effects in the transitional flow regime. The results of the computations have shown the generally good agreement with respect to the experimental measurements, in particular, the $\mathrm{Re}_{2,\mathrm{cr}}$ and the associated loss increase were well predicted.

Finally, three-dimensional unsteady computations were performed in a stage environment. The layout of the stage was selected in order to reproduce the cascade test conditions to compare the results with the cascade measurements. As for the experiments, the same five surface roughnesses and Reynolds number range were investigated. The results were also compared with the profile losses predicted by the Craig and Cox correlation, leading to two different conclusions. Similarly to the cascade environment, the stator row works in a transitional flow regime. While a different behavior is observed in the rotor row, where the incoming wakes trigger an early boundary layer transition, modifying the flow regime with respect to the cascade environment.

The results found in this work aim to have a general character. Their discussion has pointed out many aspects concerning the losses generation associated with a rough surface. Understanding these mechanisms has put the basis for tuning the roughness model used for the computations and for improving its prediction reliability. The stage environment computations highlighted that the effect of surface roughness is quite different from the one reproducible by cascade tests: the upcoming wakes on the rotor blade strongly affect the transition-related aspects and the losses associated with them. As a result, the stage environment analysis would recommend to use the best allowed surface finishing to design the blade.

Acknowledgment

The present research was carried out in the framework of a joint activity involving both industry and university members. The authors acknowledge Dr. Roberto Pacciani of University of Florence for the useful discussion on the transition/turbulence model. The authors also thank GE Oil & Gas for permission to publish this work.

Nomenclature

AR = aspect ratio $= H/C$
C = chord
C_f = skin friction coefficient, $C_\mathrm{f} = \tau_\mathrm{w}/((1/2)\rho u^2)$
H = blade height
k = turbulent kinetic energy
k_ℓ = laminar kinetic energy
k_s = equivalent sand grain roughness height
k_s^+ = roughness height in wall units, $k_\mathrm{s}^+ = k_\mathrm{s} v^*/\nu$
ℓ_T = turbulence length scale, $\ell_\mathrm{T} = k^{1/2}/\omega$
M = Mach number
P = pressure
r = radius
R_t = peak-to-valley roughness
R_y = wall-normal-distance Reynolds number, $\sqrt{k}y/\nu$
Re = Reynolds number, $\mathrm{Re} = u_2(C/\nu)$
$\mathrm{Re}_{k_\mathrm{s}}$ = roughness Reynolds number, $\mathrm{Re}_{k_\mathrm{s}} = \mathrm{Re}k_\mathrm{s}/C$
RR = radius ratio $= r_\mathrm{tip}/r_\mathrm{hub}$
S = mean shear rate $S = \sqrt{2S_{ij}S_{ij}}$
T = temperature
Tu = turbulence intensity, $Tu = \sqrt{(2/3)k}/u$
u = velocity magnitude
v^* = friction velocity, $v^* = \sqrt{\tau_\mathrm{w}/\rho}$
x, y = cartesian coordinates
y^+ = distance from the surface in wall units, $y^+ = yv^*/\nu$
Y = total pressure loss
Z_w = Zweifel number

Greek Symbols

δ_Ω = shear layer vorticity thickness, $\delta_\Omega = u_\infty/2(\partial u/\partial y)^{-1}_{\max_y}$
ν = kinematic fluid viscosity
ρ = density
τ_w = wall shear stress
ω = specific turbulence-dissipation rate

Subscripts

cr = critical
ℓ = laminar
ref = reference value
s = static
smooth = smooth surface
t = total
T = turbulent
th = threshold
w = wall value
1 = cascade inlet
2 = cascade exit
∞ = free-stream

Acronyms

CFD = computational fluid dynamics
FT = fully turbulent
LKE = laminar kinetic energy

References

[1] Nikuradse, J., 1933, "Laws for Flows in Rough Pipes," VDI-Forchungsheft 361, Series B, Vol. 4 (English translation NACA TM 1292, 1950).
[2] Schlichting, H., 1936, "Experimentelle Untersuchungen zum Rauhigkeitsproblem," Ing. Arch. **7**(1), pp. 1–34.
[3] Bons, J. P., 2010, "A Review of Surface Roughness Effects in Gas Turbines," ASME J. Turbomach., **132**(2), p. 021004.
[4] Flack, K. A., and Schultz, M. P., 2010, "Review of Hydraulic Roughness Scales in the Fully Rough Regime," ASME J. Fluid Eng., **132**(4), p. 041203.
[5] Schlichting, H., 1979, *Boundary-Layer Theory*, 7th ed., McGraw-Hill, Inc., New York.
[6] Speidel, L., 1962, "Determination of the Necessary Surface Quality and Possible Losses Due to Roughness in Steam Turbines," Elektrizitätswirtschaft, **61**(21), pp. 799–804.
[7] Hummel, F., Lötzerich, M., Cardamone, P., and Fottner, L., 2005, "Surface Roughness Effects on Turbine Blade Aerodynamics," ASME J. Turbomach., **127**(3), pp. 453–461.
[8] Dirling, R. B., 1973, "A Method for Computing Roughwall Heat Transfer Rates on Re-Entry Nosetips," AIAA Paper No. 73-763.
[9] Sigal, A., and Danberg, J. E., 1990, "New Correlation of Roughness Density Effect on the Turbulent Boundary Layer," AIAA J., **28**(3), pp. 554–556.
[10] van Rij, J. A., Belnap, B. J., and Ligrani, P. M., 2002, "Analysis and Experiments on Three-Dimensional, Irregular Surface Roughness," ASME J. Fluid Eng., **124**(3), pp. 671–677.
[11] Waigh, D. R., and Kind, R. J., 1998, "Improved Aerodynamic Characterization of Regular Three-Dimensional Roughness," AIAA J., **36**(6), pp. 1117–1119.
[12] Zhang, Q., Goodro, M., Ligrani, P. M., Trindade, R., and Sreekanth, S., 2006, "Influence of Surface Roughness on the Aerodynamic Losses of a Turbine Vane," ASME J. Turbomach., **128**(3), pp. 568–578.
[13] Im, J. H., Shin, J. H., Hobson, G. V., Song, S. J., and Millsaps, K. T., 2013, "Effect of Leading Edge Roughness and Reynolds Number on Compressor Profile Loss," ASME Paper No. GT2013-95487.
[14] Vázquez, R., and Torre, D., 2013, "The Effect of Surface Roughness on Efficiency of Low Pressure Turbines," ASME Paper No. GT2013-94200.

[15] Hodson, H. P., and Howell, R. J., 2005, "The Role of Transition in High-Lift Low-Pressure Turbines for Aeroengines," Prog. Aerosp. Sci., **41**(6), pp. 419–454.

[16] Boyle, R. J., 1994, "Prediction of Surface Roughness and Incidence Effects on Turbine Performance," ASME J. Turbomach., **116**(4), pp. 745–751.

[17] Mesbah, M., Arts, T., Simon, J. F., and Geuzaine, P., 2009, "Numerical and Experimental Analysis of Surface Roughness Effects for Compressor Blades," AIAA Paper No. ISABE-2009-1151.

[18] Boyle, R. J., and Senyitko, R. G., 2003, "Measurements and Predictions of Surface Roughness Effects on Turbine Vane Aerodynamics," ASME Paper No. GT2003-38580.

[19] Cebeci, T., and Chang, K., 1978, "Calculation of Incompressible Rough-Wall Boundary Layer Flows," AIAA J., **16**(7), pp. 730–735.

[20] Mayle, R. E., 1991, "The Role of Laminar-Turbulent Transition in Gas Turbine Engines," ASME J. Turbomach., **113**(4), pp. 509–537.

[21] Dossena, V., Perdichizzi, A., and Savini, M., 1999, "The Influence of Endwall Contouring on the Performance of a Turbine Nozzle Guide Vane," ASME J. Turbomach., **121**(2), pp. 200–208.

[22] D'Ippolito, G., Dossena, V., and Mora, A., 2011, "The Influence of Blade Lean on Straight and Annular Turbine Cascade Flow Field," ASME J. Turbomach., **133**(1), p. 011013.

[23] Speidel, L., 1954, "Einfluβ der Oberflächenrauhigkeit auf die Strömungsverluste in ebenen Schaufelgittern," Forschg, Ing.-Wes. **20**(5), pp. 129–140.

[24] Feindt, E. G., 1956, *Untersuchungen über die Abhängigkeit des Umshclages laminar-turbulent von der Oberflächenrauhigkeit und der Druckverteilung*, Springer-Verlag, Berlin.

[25] Arnone, A., Liou, M. S., and Povinelli, L. A., 1992, "Navier–Stokes Solution of Transonic Cascade Flow Using Non-Periodic c-Type Grids," J. Propul. Power, **8**(2), pp. 410–417.

[26] Arnone, A., and Pacciani, R., 1996, "Rotor-Stator Interaction Analysis Using the Navier-Stokes Equations and a Multigrid Method," ASME J. Turbomach., **118**(4), pp. 679–689.

[27] Jameson, A., 1991, "Time Dependent Calculations Using Multigrid With Applications to Unsteady Flows Past Airfoils and Wings," AIAA Paper No. 91-1596.

[28] Wilcox, D. C., 1998, *Turbulence Modeling for CFD*, 2nd ed., DCW Industries, Inc., La Cañada, CA.

[29] Mayle, R. E., and Schultz, A., 1997, "The Path to Predicting Bypass Transition," ASME J. Turbomach., **119**(3), pp. 405–411.

[30] Pacciani, R., Marconcini, M., Fadai-Ghotbi, A., Lardeau, S., and Leschziner, M. A., 2011, "Calculation of High-Lift Cascades in Low Pressure Turbine Conditions Using a Three-Equation Model," ASME J. Turbomach., **133**(3), p. 031016.

[31] Pacciani, R., Marconcini, M., Arnone, A., and Bertini, F., 2011, "An Assessment of the Laminar Kinetic Energy Concept for the Prediction of High-Lift, Low-Reynolds Number Cascade Flows," Proc. Inst. Mech. Eng. A, **225**(7), pp. 995–1003.

[32] Wilcox, D. C., 2008, "Formulation of the k-ω Turbulence Model Revisited," AIAA J., **46**(11), pp. 2823–2838.

[33] Hellsten, A., and Laine, S., 1997. "Extension of the k-ω-SST Turbulence Model for Flows Over Rough Surfaces," AIAA Paper No. 97-3577.

[34] Patel, V. C., 1998, "Perspective: Flow at High Reynolds Number and Over Rough Surfaces—Achilles Heel of CFD," ASME J. Fluid Eng., **120**(3), pp. 434–444.

[35] Knopp, T., Eisfeld, B., and Calvo, J. B., 2009. "A New Extension for k-ω Turbulence Models to Account for Wall Roughness," Int. J. Heat Fluid Flow, **30**(1), pp. 54–65.

[36] Mills, A., and Hang, X., 1983, "On the Skin Friction Coefficient for a Fully Rough Flat Plate," ASME J. Fluid Eng., **105**(3), pp. 364–365.

[37] Craig, H. R. M., and Cox, H. J. A., 1970, "Performance Estimation of Axial Flow Turbines," Proc. Inst. Mech. Eng., **185**(1), pp. 407–424.

[38] Aungier, R. H., 2006, *Turbine Aerodynamics: Axial-Flow and Radial Inflow Turbine Design and Analysis*, American Society of Mechanical Engineers, New York.